iScience

CellPress
OPEN ACCESS

Article

High-quality full-color carbon quantum dots synthesized under an unprecedentedly mild condition

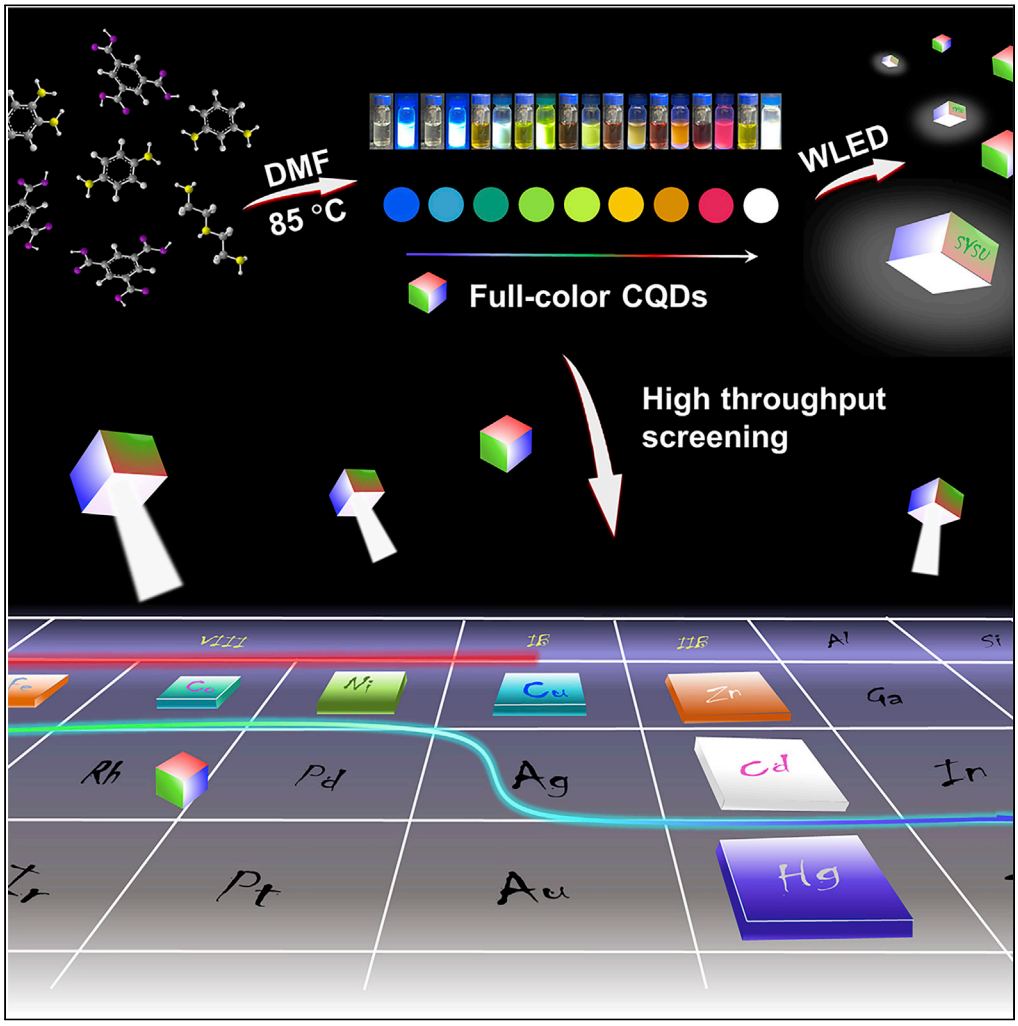

Yuan-Jun Tong, Lu-Dan Yu, Yanjun Huang, ..., Janusz Pawliszyn, Jianqiao Xu, Gangfeng Ouyang

xujq27@mail.sysu.edu.cn (J.X.)
cesoygf@mail.sysu.edu.cn (G.O.)

Highlights

High-quality full-color CQDs was fabricated under unprecedentedly mild conditions

Stable and narrow fluorescent emissions were performed with high quantum yields

LEDs with different-color and white light emissions were fabricated

Logic gate sensors that could distinguish multiple metal ions were developed

Tong et al., iScience 25, 104421
June 17, 2022
https://doi.org/10.1016/j.isci.2022.104421

iScience

CellPress
OPEN ACCESS

Article

High-quality full-color carbon quantum dots synthesized under an unprecedentedly mild condition

Yuan-Jun Tong,[1] Lu-Dan Yu,[1] Yanjun Huang,[1] Yutong Li,[1] Nan Li,[1] Qi Fu,[1] Yu-Xin Ye,[1] Fang Zhu,[1] Janusz Pawliszyn,[2] Jianqiao Xu,[1,5,*] and Gangfeng Ouyang[1,3,4,*]

SUMMARY

Carbon quantum dots (CQDs) are highly promising to be applied in light-emitting, chemosensing, and other cutting-edge domains. Herein, we successfully fabricate high-quality full-color CQDs under unprecedentedly low temperature and pressure (85°C, 1.88 bar). Stable and narrow fluorescent emissions ranging from blue to green and red light were realized by simple amine engineering, which were further mixed into white-light CQDs with the absolute photoluminescent quantum yield reaching 19.2%. The average mass yield of the CQDs reached 69.0%. The optical performances demonstrated that the CQDs possessed uniform luminescent centers and dominant radiative decay channels. Component analysis further suggested that dehydrated condensation between carboxyl and amine groups directed the growth of the CQDs. By utilizing the CQDs, full-color light-emitting diodes and logic gate sensors were developed. This study paves an important step for promoting the application of CQDs by providing an energy-efficient, safe, and productive synthetic strategy.

INTRODUCTION

The discovery of room temperature light emission from quantum-sized carbon (<10 nm) in 2006 has triggered intensive research on light-emitting carbon quantum dots (CQDs) (Sun et al., 2006). The tunability of their photoluminescent spectra and their surface chemistry make them highly potential candidates to be used in light-emitting, chemosensing, and other domains (Wang et al., 2017, 2020; Jiang et al., 2015; Li et al., 2017). Moreover, CQDs also outperform many other fluorescent nanomaterials in term of their high stability and environmental friendliness (Chung et al., 2020; Shi et al., 2021; Zhu et al., 2013; Huang et al., 2012; Yuan et al., 2019; Vasilopoulou et al., 2020).

Plenty of studies have been devoted to developing novel methods for the synthesis of high-quality photoluminescent CQDs, which are unexceptionally classified as "top-down" or "bottom-up" methods (Semeniuk et al., 2019; Nekoueian et al., 2019; Wareing et al., 2021; Briscoe et al., 2015). For a "top-down" method, CQDs are synthesized by breaking down larger carbon materials such as graphite that contain abundant sp^2-hybridized carbon atoms, via arc discharge, laser ablation, and other energy-intensive strategies (Chung et al., 2021; Xu et al., 2013). On the other hand, high temperature, high pressure, and/or strong oxidative reagents are usually requested for the "bottom-up" synthesis of CQDs from small molecular precursors such as carbohydrates and amino acids, for the purpose of carbonizing the sp^3 carbon to sp^2 carbon (Mosconi et al., 2015; Li et al., 2021; Ding et al., 2016; Baragau et al., 2020, 2021). Thus, hydrothermal and solvothermal reactions are frequently adopted in "bottom-up" methods. Besides the high energy consumption in these methods, the harsh synthetic conditions also raise the concerns on the safety of the methods and decrease the productivity by transforming the precursors partially to gaseous byproducts.

Up to now, the development of synthetic methods that are energy efficient, safe, and highly productive for CQDs is still on the way, which would be of great value for promoting the applications of CQDs in industry, by circumventing complicated production facilities and high energy input. Even the electrochemical methods are much greener and safer than their counterparts (Wang et al., 2014), and extra separation steps for obtaining optically homogeneous CQDs are required (Bao et al., 2011). Besides, the recently reported

[1]MOE Key Laboratory of Bioinorganic and Synthetic Chemistry/KLGHEI of Environment and Energy Chemistry, School of Chemistry, Sun Yat-sen University, Guangzhou, Guangdong 510275, P. R. China

[2]Department of Chemistry, University of Waterloo, Waterloo, Ontario N2L3G1, Canada

[3]Chemistry College, Center of Advanced Analysis and Gene Sequencing, Zhengzhou University, Kexue Avenue 100, Zhengzhou 450001, China

[4]Guangdong Provincial Key Laboratory of Emergency Test for Dangerous Chemicals, Guangdong Institute of Analysis (China National Analytical Center Guangzhou), Guangdong Academy of Sciences, 100 Xianlie Middle Road, Guangzhou 510070, China

[5]Lead contact

*Correspondence: xujq27@mail.sysu.edu.cn (J.X.), cesoygf@mail.sysu.edu.cn (G.O.)

https://doi.org/10.1016/j.isci.2022.104421

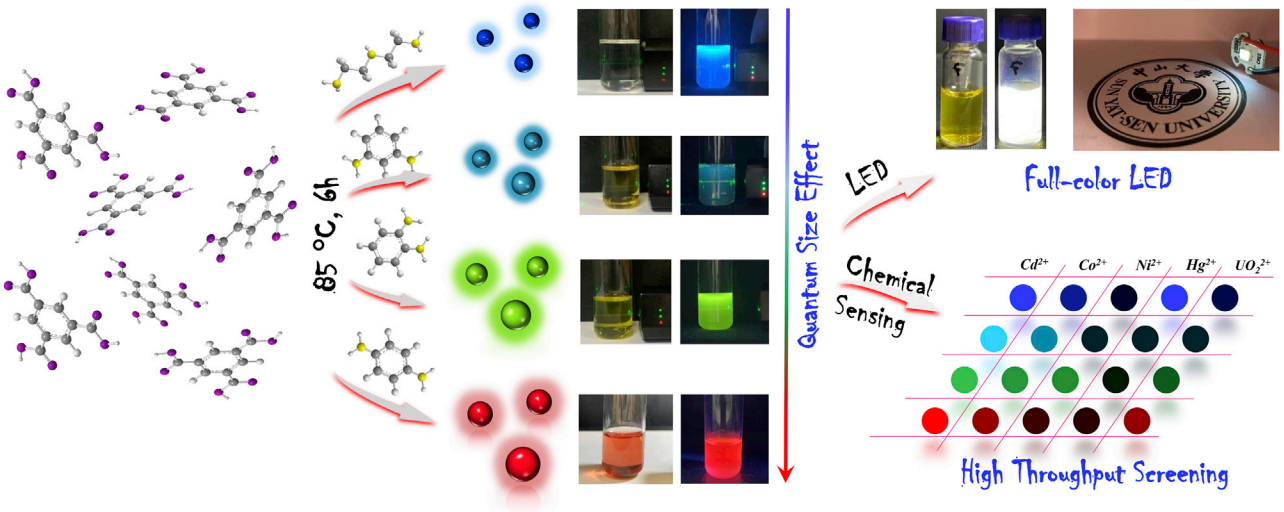

Figure 1. The procedures for the preparation of full-color CQDs and its application in LEDs and chemosensing.

mild "bottom-up" methods by using phenols and ethylenediamine/diethylenetriamine as the precursors only produced blue and green CQDs (An et al., 2021; Liu et al., 2020; Zhang et al., 2018).

Herein, we develop a mild condensation strategy to produce high-quality full-color CQDs (Figure 1). 1,3,5-benzenetricarboxylic acid (BTCA) that contains only sp^2 carbon is chosen as the acid reagent, whereas diethylenetriamine (DETA), *m*-phenylenediamine (mPDA), *o*-phenylenediamine (oPDA), and *p*-phenylenediamine (pPDA) are used as the basic reagents. Different from the hydrothermal and solvothermal methods that relied on high temperature (180–250°C) and high pressure (up to 248 bar) (Baragau et al., 2020, 2021), our one-pot method was conducted at 85°C and nearly atmospheric pressure (about 1.88 bar). The fluorescent spectra of the obtained CQDs were successfully modulated over a wide range from blue to red by amine engineering. And white light emission was obtained by mixing the CQDs. The absolute fluorescence quantum yield (QYs) reached 19.2% for the white CQDs, and the average mass yield of the CQDs reached 69.0%. Moreover, owing to the high luminescence and the diversified color of the CQDs, light-emitting diodes (LEDs) with different-color and white light emission were fabricated, and logic gate sensors that could distinguish multiple metal ions with high accuracy were developed.

RESULTS AND DISCUSSION

Preparation and optical properties of the CQDs

Different from the traditional methods using carbohydrate, amino acids, or citrate as precursors, precursors containing only sp^2 carbon were first selected for the synthesis of CQDs in this study, by excluding the need for carbonizing the sp^3 carbon into sp^2 carbon. BTCA was selected as the acidic reagent, and mPDA, oPDA, and pPDA were chosen as the basic reagents. The reactions were performed by heating the mixture of BTCA and one of the selected bases in N,N-dimethylformamide (DMF) in glass bottles under 85°C for only 6 h, which was far below the temperatures in hydrothermal and solvothermal reactions (Wang et al., 2017, 2020; Ding et al., 2016; Qin et al., 2019; Meng et al., 2021; Liu et al., 2012; Yuan et al., 2018). Three CQDs that presented bright blue, green, and red light emission bands centered at about 440, 550, and 605 nm, respectively, were obtained (Figures 2A–2C). The three CQDs were termed *m*-bCQDs, *o*-gCQDs, and *p*-rCQDs, respectively.

For comparison, a range of amines containing sp^3 carbon were also selected as the basic reagents (Figure S1). Most of the as-prepared solutions emitted very weak blue fluorescence except for that of DETA, which emitted even the strongest blue light among all the blue light emitters (termed d-bCQDs, fluorescent band centered over 430 nm; Figures 2D and S2). Thus, DETA together with the other three phenylenediamines were used for the synthesis of CQDs in the followed experiment. It is notable that the use of DETA and another precursor containing only sp^2 carbon (*p*-aminophenol) in preparing bright blue CQDs under mild conditions also succeeded before (An et al., 2021).

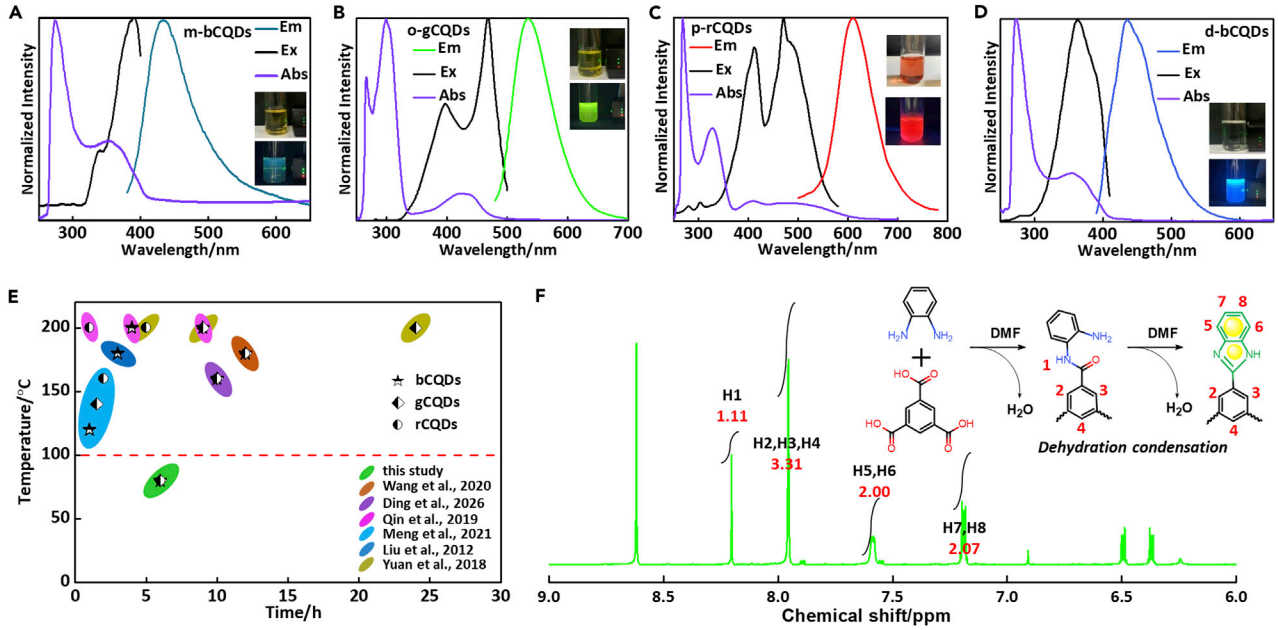

Figure 2. Optical properties, comparison data, and synthesis route of the CQDs

(A) Excitation, emission, and UV-adsorption spectra of *m*-bCQDs. Inset: corresponding photos of the CQDs with Tyndall effect observed.

(B) Excitation, emission, and UV-adsorption spectra of *o*-gCQDs. Inset: corresponding photos of the CQDs with Tyndall effect observed.

(C) Excitation, emission, and UV-adsorption spectra of *p*-rCQDs. Inset: corresponding photos of the CQDs with Tyndall effect observed.

(D) Excitation, emission, and UV-adsorption spectra of d-bCQDs. Inset: corresponding photos of the CQDs with Tyndall effect observed.

(E) Comparison with other synthetic methods for CQDs.

(F) Supposed dehydrated condensation route of *o*-gCQDs and the assignment of the ^{1}HNMR signals for *o*-gCQDs.

To obtain the optimal reaction conditions, the effect of the solvent was first explored. It was observed that high-quality and diversified photoluminescence could only be achieved by using DMF as the solvent (Figure S3), which might be attributed to the higher basicity of DMF. Subsequently, the reaction temperature, time, and ratios of precursors were investigated thoroughly (Figures S4, S5 and S6, text S1.4). It was found that reacting at 85°C for 6 h was the optimal condition for d-bCQDs, *m*-bCQDs, and *o*-gCQDs and also produced satisfying *p*-rCQDs (Figure S4). At lower temperature, the growth of CQDs seemed to be much slower, whereas at higher temperature, the growth might be too fast to form the high-quality emitting centers of the CQDs. Besides, it was not commentary to significantly extend the reaction time, as the overgrowth might lead to products exceeding the quantum sizes.

As far as we know, full-color CQDs were scarcely prepared under 100°C by using any other "bottom-up" methods (Figure 2E) (Wang et al., 2020; Ding et al., 2016; Qin et al., 2019; Meng et al., 2021; Liu et al., 2012; Yuan et al., 2018). The temperature was even far below the boiling point of the solvent, which left the pressure estimated to be 1.88 bar (text S1.3). The low pressure could be borne by glass sample bottles, in sharp contrast to the high pressures in the hydrothermal and solvothermal processes that can only be borne by autoclaves. The relative low temperature and pressure are highly beneficial for the practical application of the CQDs, as complicated facilities and high energy input can be circumvented for their production.

Moreover, the average mass yield of the CQDs reached 69.0% (Table S1), which was comparable to previous work (Meng et al., 2021). The absolute photoluminescent quantum yield for d-bCQDs, *m*-bCQDs, *o*-gCQDs, and *p*-rCQDs was determined to be 35.3%, 0.6%, 16%, and 7.9% (Figure S7). And it was found the CQDs kept high photoluminescent stability under a long-term excitation (Figure S8) and presented good reproducibility among different batches, which also demonstrated the capacities of the CQDs for practical application.

Furthermore, the optical performances of the CQDs were investigated in details. The gradually redshifted fluorescent bands were consistent with the redshifted absorption bands, and the position of the excitation

peak was quite close to that of the absorption band in the lower energy region (Figures 1A–1D), implying that the fluorescence of the CQDs was clearly originated from the photon absorption in the lower-energy region. The maximum emission wavelengths were nearly independent of the excitation wavelengths (Figure S9), which were dissimilar to that of the excitation-dependent emissions of many other CQDs (Qin et al., 2019), and suggested the existence of dominant luminescent centers in each type of the present CQDs (Ding et al., 2016). In addition, the mono-exponential decay characteristics of the fluorescence lifetime once again demonstrated that there existed a dominant radiative channel in each type of the CQDs (Figure S10) (Qin et al., 2019). Besides, the CQDs exhibited satisfying color purities, and the full width at half maximum (FWHM) of the emission bands were all smaller than 80 nm (70 nm–78 nm, Table S2), which also demonstrated the narrowly dispersed band gaps of the luminescent centers and the negligible competitive decay channels (Yuan et al., 2018). Taken all together, it could be inferred that each type of the CQDs possessed relatively uniform morphologies and surface states, and the defects in the CQDs might either be negligible or play little effects in the decay processes (Ding et al., 2016; Yuan et al., 2018).

Structure analysis

To further elucidate the compositions and structures of the CQDs (Figure S11), ^{1}HNMR analysis was first adopted. Taking *o*-gCQDs as an example, in the as-synthetic product, the signals of excessive BTCA (8.61 ppm) and oPDA (6.35 ppm–6.55 ppm) were observed (Figure S12). Moreover, some of the characteristic proton signals of the benzimidazole were appeared (7.19 and 7.59 ppm); thus, benzimidazole moieties were supposed to be formed in *o*-gCQDs. Another two new singlet peaks appeared in high field, the peak with larger integration result was assigned to the condensed BTCA moieties (7.95 ppm), and the other peak was assigned to the imide moieties (8.20 ppm). Except for the characteristic proton peaks, some of the integral peak area of the proton signals presented good ratio relationship (Figure 2F), which further suggested the dehydrate condensation between the carboxyl and amine groups (Figure S12). Similar to *o*-gCQDs, imide groups were plausibly identified in d-bCQDs, *m*-bCQDs, and *p*-rCQDs (Figures S13, S14 and S15).

Moreover, these CQDs exhibited similar Fourier transform infrared (FTIR) spectra (Figure S16). The strong vibration bands of C=N were observed at 1510 cm^{-1} (Chen et al., 2021; Weetman et al., 2019). Bands at 3435, 1651, 1380, and 1100 cm^{-1} were ascribed to the stretching vibration of N-H, C=O, C-N, and C-O (An et al., 2021; Chen et al., 2021), respectively, which also demonstrated that the dehydrate condensation occurred between the carboxyl and amine groups. X-ray photoelectron spectroscopy (XPS) further verified the presence of carboxyl and amine in the CQDs (Figure S17) (Weetman et al., 2019). Moreover, the thermogravimetric analysis also indicated the containing of oxygen- and nitrogen-containing groups within the CQDs (Figure S18). When the temperature reached about 120°C, weight losses up to 8% were observed, which should be attributed to the evaporation of solvent (H_2O and DMF). Subsequently, the weight losses of the CQDs above 120°C could be attributed to the decomposition of oxygen- and nitrogen-containing groups. Even being heated to 450°C, the weight losses were all less than 30%. The residues at 450°C should be attributed to the carbon cores of the CQDs. These data demonstrated that dehydrate condensation played an important role in the growth of these CQDs, as speculated in Figure S11. The dehydrate reactions other than extensive carbonization might be the reason for the succeeded synthesis of the CQDs under the mild reaction conditions. It is also highly notable that the mild synthetic method was beneficial for resolving the structures and condensation routes of the CQDs, as complex carbonization processes could be excluded.

In addition, as shown in Figure 3, all of these CQDs showed narrow size distribution with the average sizes of about 2.2 nm (d-bCQDs), 2.5 nm (*m*-bCQDs), 2.9 nm (*o*-gCQDs), and 3.4 nm (*p*-rCQDs), respectively. The high-resolution transmission electron microscopic (HRTEM) images further showed the in-plane lattice spacing of graphene (100 facet) in all the CQDs (Figures 3E–3H). X-ray powder diffraction (XRD) patterns around 25° corresponded to the (002) layer spacing of graphene in all the CQDs (Figure S19). AFM revealed that the heights were in the range from 1 to 2 nm, elucidating that they consisted of two–five layers of graphene. Besides, the matrix-assisted laser desorption/ionization-mass spectrometry (MALDI-MS) showed that the ions of CQDs were distributed in the mass-to-charge ratio range from 330 to 1500 (Figure S20). And from d-bCQDs, *m*-bCQDs, *o*-gCQDs, to *p*-rCQDs, the mass-to-charge ratios gradually increased, which was well consistent with the increasing of the overall sizes of the CQDs. The gradually increased sizes of the CQDs were consistent with the redshifted fluorescence and the redshifted absorption bands, which demonstrated the quantum confinement effect was probably embedded behind the redshifted spectra.

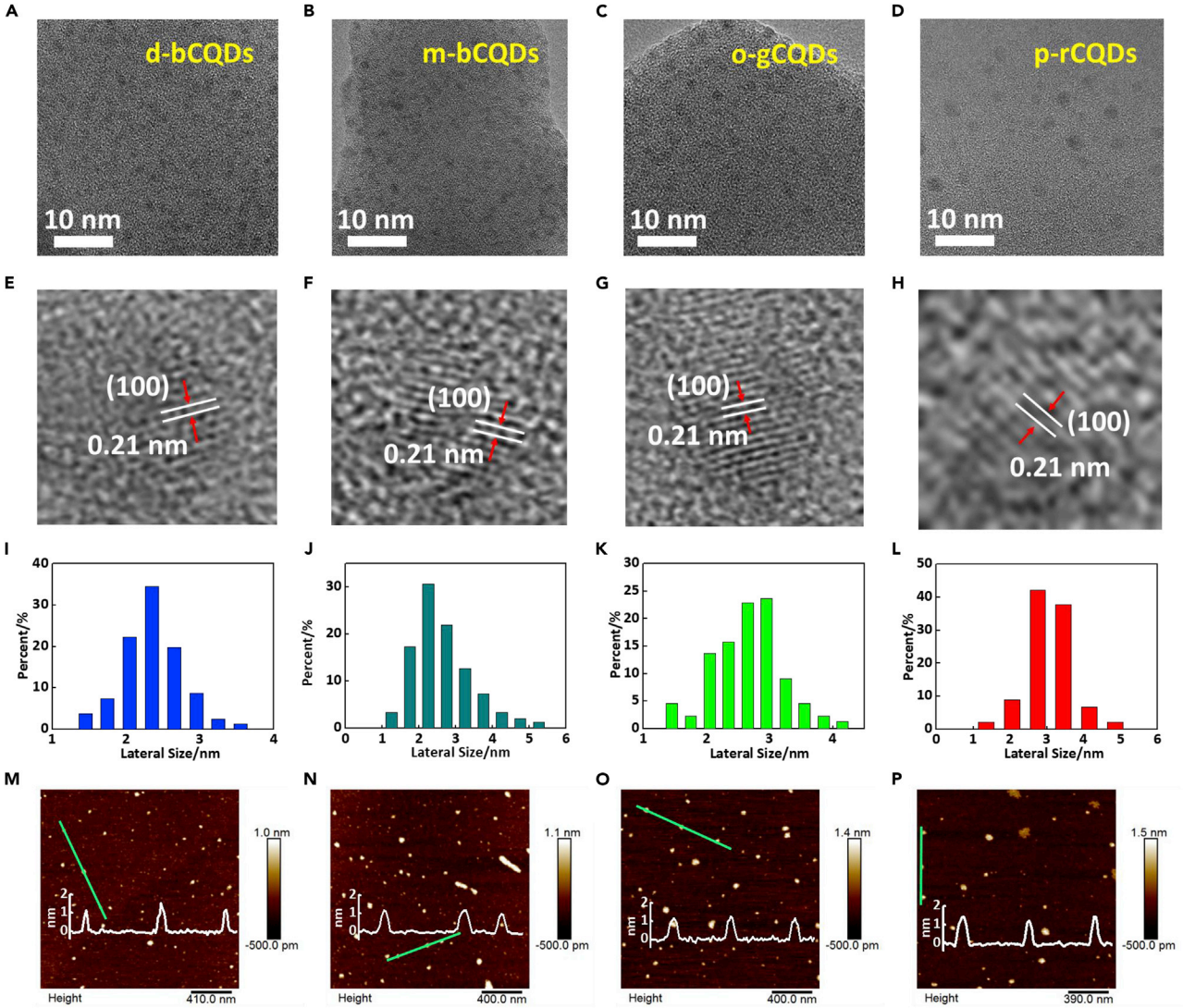

Figure 3. TEM and AFM characterization of the CQDs

(A) TEM image of d-bCQDs.
(B) TEM image of *m*-bCQDs.
(C) TEM image of *o*-gCQDs.
(D) TEM image of *p*-rCQDs.
(E) Highlighted lattice image of d-bCQDs.
(F) Highlighted lattice image of m-bCQDs.
(G) Highlighted lattice image of o-gCQDs.
(H) Highlighted lattice image of p-rCQDs.
(I) Statistically derived size distributions of d-bCQDs from its TEM image.
(J) Statistically derived size distributions of *m*-bCQDs from its TEM image.
(K) Statistically derived size distributions of *o*-gCQDs from its TEM image.
(L) Statistically derived size distributions of *p*-rCQDs from its TEM image.
(M) AFM image of d-bCQDs.
(N) AFM image of *m*-bCQDs.
(O) AFM image of *o*-gCQDs.
(P) AFM image of *p*-rCQDs.

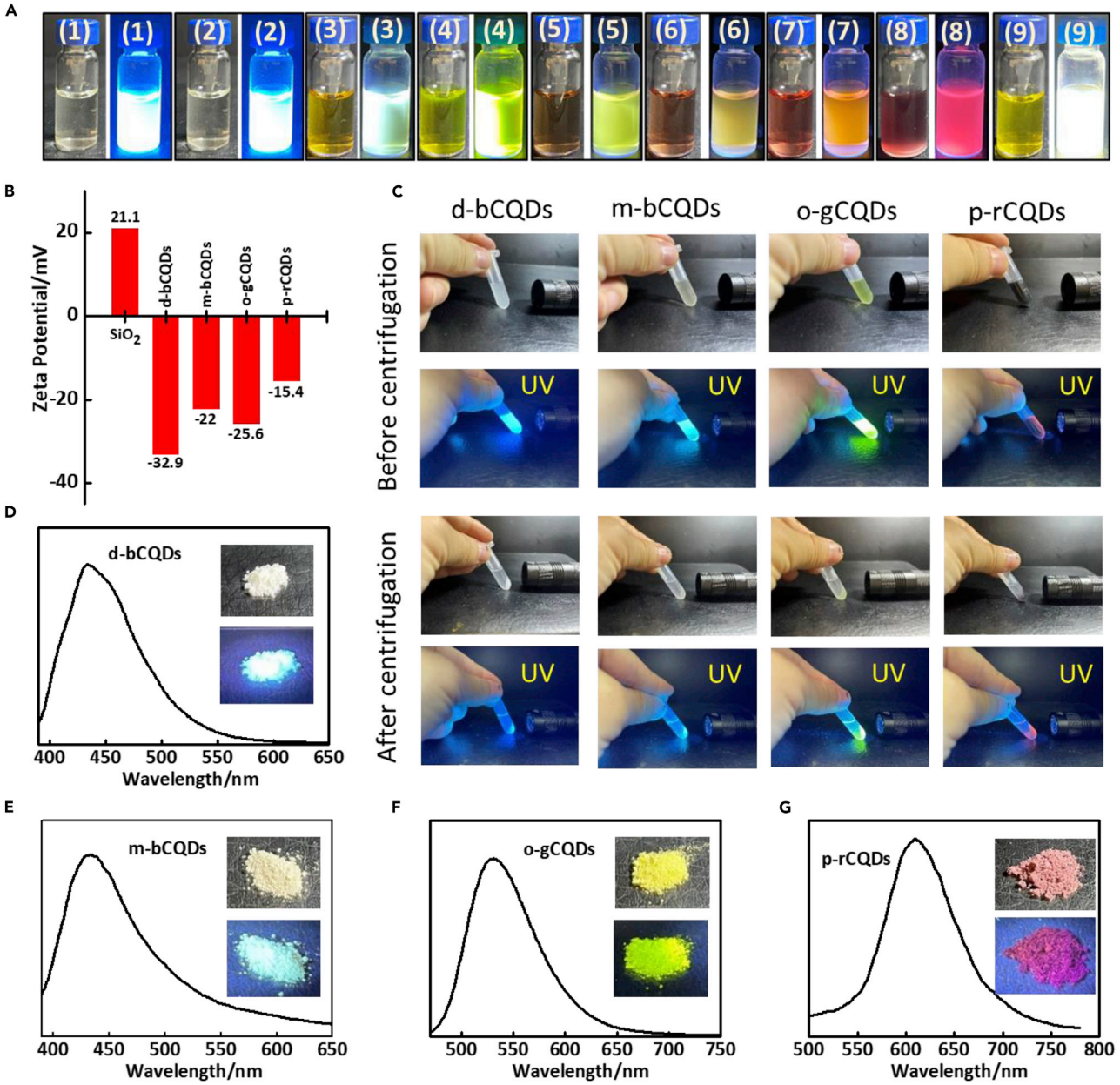

Figure 4. Preparation and deposition of full-color CQDs

(A) Photos of CQDs mixtures at different volume ratios under sunlight and UV light (365 nm). (1) d-bCQDs, (2) d-bCQDs/o-gCQDs = 2:1, (3) d-bCQDs/o-gCQDs = 1:2, (4) *o*-gCQDs, (5) *o*-gCQDs/p-rCQDs = 2:1, (6) *o*-gCQDs/p-rCQDs = 1:1, (7) *o*-gCQDs/p-rCQDs = 1:2, (8) *p*-rCQDs, (9) wCQDs.

(B) Zeta potentials of SiO_2 microparticles, d-bCQDs, *m*-bCQDs, *o*-gCQDs, and *p*-rCQDs, respectively.

(C) Photos of d-bCQDs, *m*-bCQDs, *o*-gCQDs, and *p*-rCQDs mixed with SiO_2 before and after centrifugation under sunlight and UV light (365 nm).

(D) Fluorescent spectra of solid-state d-bCQDs. Inset: photos of solid-state d-bCQDs.

(E) Fluorescent spectra of solid-state *m*-bCQDs. Inset: photos of solid-state *m*-bCQDs.

(F) Fluorescent spectra of solid-state *o*-gCQDs. Inset: photos of solid-state *o*-gCQDs.

(G) Fluorescent spectra of solid-state *p*-rCQDs. Inset: photos of solid-state *p*-rCQDs.

Meanwhile, the emission spectra were also redshifted along with the increase of the C-N/C=N ration and the positive shifts of the Zeta potentials (Figures S17 and 4B), which indicated the surface states might also be involved in the emission efficiency. When triggered by different pH and different target ions, the photoluminescent intensities of the CQDs were changed, whereas the maximum emission wavelengths remained nearly constant (Figures S21 and S22). Thus, it was believed that the fluorescence of the CQDs origins from

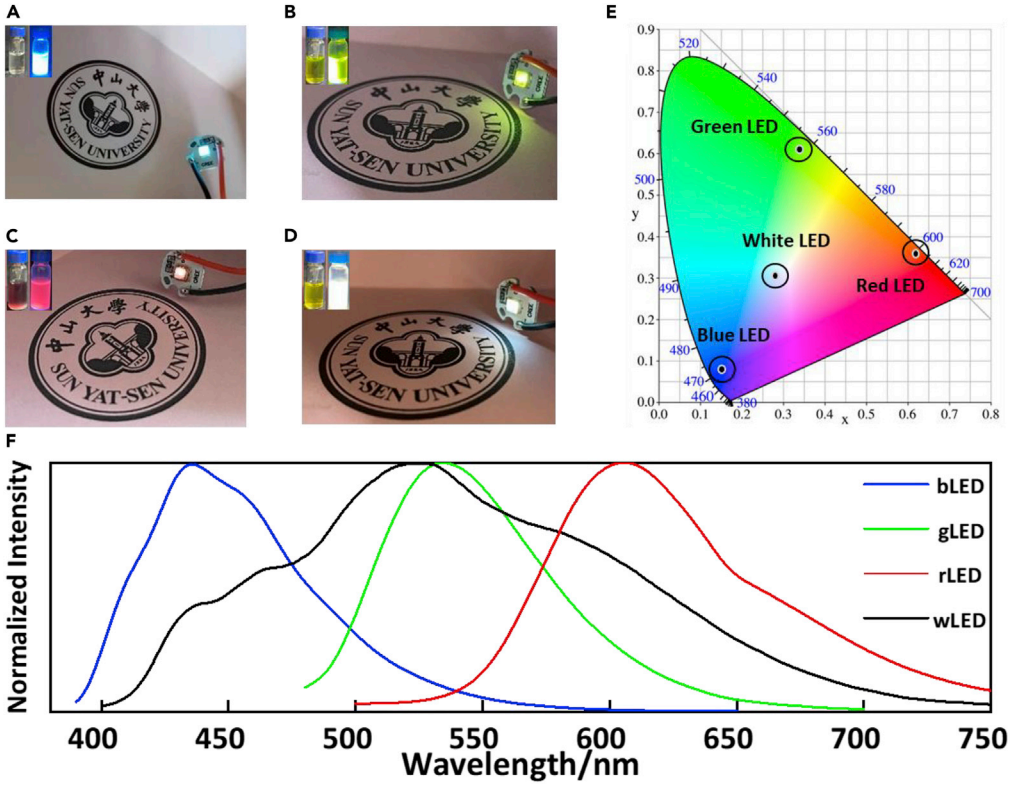

Figure 5. Photos of full-color CQDs and its application in LEDs

(A) Photo of d-bCQDs-based LED chip.

(B) Photo of *o*-gCQDs-based LED chip.

(C) Photo of *p*-rCQDs-based LED chip.

(D) Photo of wCQDs-based LED chip.

(E) CIE chromaticity coordinate of d-bCQDs, *o*-gCQDs, *p*-rCQDs, and wCQDs.

(F) Emission spectra of the LEDs of d-bCQDs, *o*-gCQDs, *p*-rCQDs, and wCQDs.

the surface states and the energy gaps of the surface emissive sites were determined by both the sizes of the π-electron systems and the surface chemistries. Similar mechanism was also reported before (Bao et al., 2015; Liu et al., 2018). To further verify this proposal, H_2O_2 was mixed with the CQDs. It was observed that the emission intensities of CQDs decreased, but the emission wavelengths only shifted slightly (Figure S23). In such case, surface functional groups of CQDs were oxidized but the carbon cores were insusceptible to the damage.

Full-color CQDs preparation and application in LEDs

By mixing the solutions of d-bCQDs, *o*-gCQDs, and *p*-rCQDs at different volume ratios, various photoluminescent colors including blue, cyan, green, orange, red, and even white were created (Figures 4A and S24). The QY reached 19.2% for the white CQDs from this facile strategy, which is comparable to most of the reported CQDs that depended on other harsh preparation methods (Wang et al., 2020; Ding et al., 2016; Qin et al., 2019; Meng et al., 2021; Liu et al., 2012; Yuan et al., 2018). To further obtain solid-state CQDs, an electrostatic deposition method was used to deposit the CQDs on positively charged SiO_2 microparticles (modified with APTES), as the CQDs exhibited negative Zeta potentials that were attributed to the excessive carboxyl groups (Figures S16 and 4B). The value of the Zeta potential of the positively charged SiO_2 was +21.1 mV, whereas the Zeta potentials were −32.9, −22, −25.6, and −15.4 mV for d-bCQDs, *m*-bCQDs, *o*-bCQDs, and *p*-rCQDs, respectively. The SiO_2 micropaticles were firstly well dispersed in the solution of the CQDs and then centrifuged. Almost all the CQDs were precipitated along with SiO_2 after centrifugation (Figure 4C). The dried powders exhibited the characteristic fluorescence emission bands of each CQDs. The solid-state CQDs displayed fluorescent emission spectra similar to the CQDs solution (Figures 4D–4G).

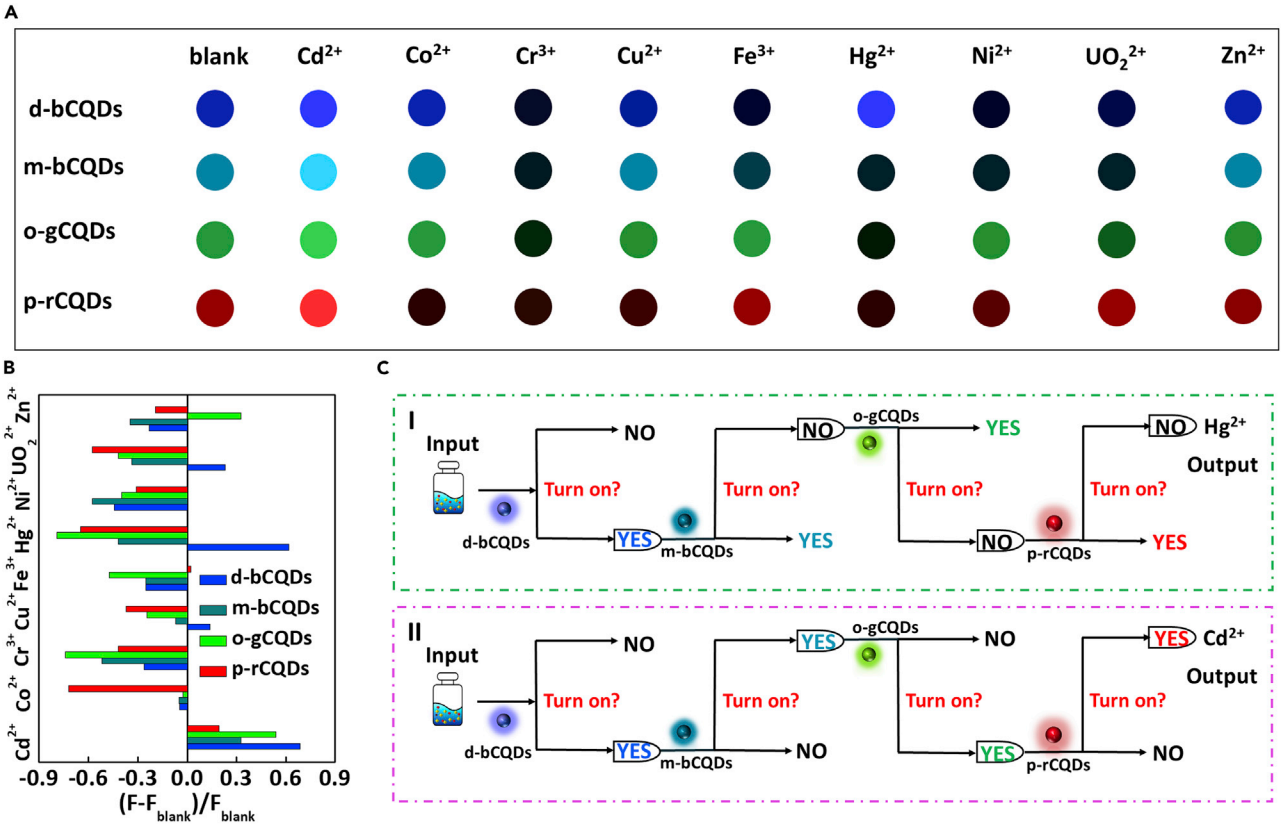

Figure 6. Application in chemical sensing

(A) Photos of d-bCQDs, *m*-bCQDs, *o*-gCQDs, and *p*-rCQDs treated with ions (1 mg L^{-1}) under UV light (365 nm).

(B) The biased ratios of the fluorescent intensities after treated with different ions (1 mg L^{-1}), respectively.

(C) The CQDs-based AND logic gates for identifying (I) Hg^{2+} and (II) Cd^{2+}.

On the basis of the excellent fluorescent emission, the solid-state CQDs were successfully prepared into bright and uniform full-color light-emitting diodes (LEDs). Figures 5A–5C displayed the close-up view of the obtained LEDs with surface emission from blue and green to red emission of CQDs-based monochrome LEDs. The CIE coordinates of the emitted lights of these LEDs were (0.17, 0.1), (0.29, 0.6), and (0.61, 0.41) (Figure 5E), respectively. The emission spectra of the LEDs were shown in Figure 5F. By combining the d-bCQDs, *o*-gCQDs, and *p*-rCQDs with the ratio of 1:2:3 (V/V/V), the white LED with the CIE color coordinate (0.27, 0.31) has also been achieved (Figure 5D). The emission spectrum of the white LED covered the whole visible light region from 400 to 750 nm (Figure 5F). The full-color LEDs demonstrated that the CQDs were promising candidates for display and lighting.

Application in chemical sensing

It was found that the fluorescence of the CQDs could be tuned by pH and metal ions, as protonation/deprotonation and coordination sites, i.e. carboxyl groups and amino groups (Figures S21, S22 and 4B). Hence the CQDs could be further used for sensing pH and multiple metal ions (Figures 6, S21 and S22). The CQDs showed monotonous responses to pH in the range from 2.2 to 11 (Figure S21). The relative changes of the fluorescent intensities of d-bCQDs, *m*-bCQDs, *o*-gCQDs, and *p*-rCQDs after treated with ions were shown in Figure 6B. The different responding patterns demonstrated that the four CQDs could be used as a fluorescent array for distinguishing metal ions. The inner-filter effect was obviously insufficient to explain the responses (Figure S25), and the embedded mechanisms may need detailed studies in the future. Still, these disparate responses illustrated that the CQDs possessed rich response mechanisms, which provided a valuable chance to construct high-throughput devices for environmental analysis, medical diagnosis, food analysis, and other applications. Inspired by these responses to metal ions,

CQDs-based logic gate sensors could be further constructed. Take Hg^{2+} and Cd^{2+} as two examples, d-bCQDs, *m*-bCQDs, *o*-gCQDs, and *p*-rCQDs formed logic gates (Figure 6C).

CONCLUSIONS

In summary, developing energy-efficient, safe, and productive synthetic methods for full-color CQDs is crucial for their further success in LEDs, chemical sensing, and other applications. In this study, we report a new method in glass bottles under low pressure (1.88 bar) and with the reaction temperature as low as 85°C. The obtained CQDs possessed high QYs, high productivities, uniform luminescent centers, and dominant radiative decay channels. Besides, the mild reaction condition also made it possible to resolve the structures and condensation routes of the CQDs in depth. Full-color LEDs and logic gate sensors were developed based on the obtained high-quality CQDs. This study paves an important step for promoting the application of CQDs by providing an unprecedentedly mild synthetic strategy for full-color CQDs. This study also inspires the development of other mild synthetic methods that leave the structures of CQDs fully resolvable in the future, which is invaluable for building clear structure-property relationship and tuning photoluminescent properties at molecular accuracy.

Limitations of the study

Full-color CQDs were fabricated under mild conditions with the average mass yield reaching 69.0%. In the follow-up research, it is expected to further elucidating the growth mechanism by using sophisticated structural analytical techniques such as scanning tunneling microscopy (STM).

STAR★METHODS

Detailed methods are provided in the online version of this paper and include the following:

- KEY RESOURCES TABLE
- RESOURCE AVAILABILITY
  - Lead contact
  - Materials availability
  - Data and code availability
- EXPERIMENTAL MODEL AND SUBJECT DETAILS
- METHOD DETAILS
  - Preparation of CQDs
  - Preparation of CQDs with different ratios of precursors
  - QY measurement
  - LED fabrication
  - Procedures for sensing metal ions
  - Reaction pressure calculation
- QUANTIFICATION AND STATISTICAL ANALYSIS
- ADDITIONAL RESOURCES

SUPPLEMENTAL INFORMATION

Supplemental information can be found online at https://doi.org/10.1016/j.isci.2022.104421.

ACKNOWLEDGMENTS

Thanks for the support of National Key Research and Development Program of China (2017YFE0133200), National Natural Science Foundation of China (22122612, 22036003, 21806188 and 22076222), NSF of Guangdong Province (2018A030313324), Guangzhou Science and technology planning project (202102020329, 201803030018), the NSF of Guangdong Provincial Key R&D Program (2020B1111350002), and the Fundamental Research Funds for the Central Universities (2021qntd24).

AUTHOR CONTRIBUTIONS

Y.-J. Tong prepared the materials, studied the fluorescent properties, and wrote the manuscript; L.-D. Yu, Y. Huang, and Q. Fu helped with the study on the fluorescent properties; N. Li, Y. Li, and Y. Ye helped with the characterizations of AFM, TEM, and FTIR; J. Xu designed the experiment and helped with the funding acquisition and supervision. F. Zhu, J. Pawliszyn, and G. Ouyang helped with project administration, review, and editing.

DECLARATION OF INTERESTS

The authors declare no competing interests.

Received: January 12, 2022
Revised: April 25, 2022
Accepted: May 12, 2022
Published: June 17, 2022

REFERENCES

Alaş, M.Ö., and Genç, R. (2021). Solvatochromic surface-passivated carbon dots for fluorometric moisture sensing in organic solvents. ACS Appl. Nano Mater. *4*, 7974–7987. https://doi.org/10.1021/acsanm.1c01282.

An, J., Hu, Y., Liu, G., Che, M., Chen, R., Lyu, Y., Yuan, M., Luo, M., and Liu, Y. (2021). A fluorometric and colorimetric dual-signal nanoplatform for ultrasensitive visual monitoring of the activity of alkaline phosphatase. J. Mater. Chem. B *9*, 2998–3004. https://doi.org/10.1039/d0tb02531c.

Bao, L., Zhang, Z.-L., Tian, Z.-Q., Zhang, L., Liu, C., Lin, Y., Qi, B., and Pang, D.-W. (2011). Electrochemical tuning of luminescent carbon nanodots: from preparation to luminescence mechanism. Adv. Mater. *23*, 5801–5806. https://doi.org/10.1002/adma.201102866.

Bao, L., Liu, C., Zhang, Z.-L., and Pang, D.-W. (2015). Photoluminescence-tunable carbon nanodots: surface-state energy-gap tuning. Adv. Mater. *27*, 1663–1667. https://doi.org/10.1002/adma.201405070.

Baragau, I.-A., Power, N.P., Morgan, D.J., Heil, T., Lobo, R.A., Roberts, C.S., Titirici, M.-M., Dunn, S., and Kellici, S. (2020). Continuous hydrothermal flow synthesis of blue-luminescent, excitation-independent nitrogen-doped carbon quantum dots as nanosensors. J. Mater. Chem. *8*, 3270–3279. https://doi.org/10.1039/c9ta11781d.

Baragau, I.-A., Power, N.P., Morgan, D.J., Lobo, R.A., Roberts, C.S., Titirici, M.-M., Middelkoop, V.A., Diaz, S., Dunn, S., and Kellici, S. (2021). Efficient continuous hydrothermal flow synthesis of carbon quantum dots from a targeted biomass precursor for on–off metal ions nanosensing. ACS Sustain. Chem. Eng. *9*, 2559–2569. https://doi.org/10.1021/acssuschemeng.0c08594.

Briscoe, J., Marinovic, A., Sevilla, M., Dunn, S., and Titirici, M. (2015). Biomass-derived carbon quantum dot sensitizers for solid-state nanostructured solar cells. Angew. Chem. Int. Ed. Engl. *54*, 4463–4468. https://doi.org/10.1002/anie.201409290.

Chen, J., Zhu, Q., Jiang, L., Liu, R., Yang, Y., Tang, M., Wang, J., Wang, H., and Guo, L. (2021). Rechargeable aqueous aluminum organic batteries. Angew. Chem. Int. Ed. Engl. *60*, 5794–5799. https://doi.org/10.1002/anie.202011144.

Chung, Y.J., Kim, J., and Park, C.B. (2020). Photonic carbon dots as an emerging nanoagent for biomedical and healthcare applications. ACS Nano *14*, 6470–6497. https://doi.org/10.1021/acsnano.0c02114.

Chung, S., Revia, R.A., and Zhang, M. (2021). Graphene quantum dots and their applications in bioimaging, biosensing, and therapy. Adv. Mater. *33*, 1904362. https://doi.org/10.1002/adma.201904362.

Ding, H., Yu, S.B., Wei, J.S., and Xiong, H.M. (2016). Full-color light-emitting carbon dots with a surface-state-controlled luminescence mechanism. ACS Nano *10*, 484–491. https://doi.org/10.1021/acsnano.5b05406.

Huang, P., Lin, J., Wang, X., Wang, Z., Zhang, C., He, M., Wang, K., Chen, F., Li, Z., Shen, G., et al. (2012). Light-triggered theranostics based on photosensitizer-conjugated carbon dots for simultaneous enhanced-fluorescence imaging and photodynamic therapy. Adv. Mater. *24*, 5104–5110. https://doi.org/10.1002/adma.201200650.

Jia, H., Wang, Z., Yuan, T., Yuan, F., Li, X., Li, Y., Tan, Z., Fan, L., and Yang, S. (2019). Electroluminescent warm white light-emitting diodes based on passivation enabled bright red bandgap emission carbon quantum dots. Adv. Sci. *6*, 1900397. https://doi.org/10.1002/advs.201900397.

Jiang, K., Sun, S., Zhang, L., Lu, Y., Wu, A., Cai, C., and Lin, H. (2015). Red, green, and blue luminescence by carbon dots: full-color emission tuning and multicolor cellular imaging. Angew. Chem. Int. Ed. Engl. *54*, 5360–5363. https://doi.org/10.1002/ange.201501193.

Li, F., Li, T., Sun, C., Xia, J., Jiao, Y., and Xu, H. (2017). Selenium-Doped carbon quantum dots for free-radical scavenging. Angew. Chem. Int. Ed. Engl. *129*, 10042–10046. https://doi.org/10.1002/ange.201705989.

Li, L., Li, Y., Ye, Y., Guo, R., Wang, A., Zou, G., Hou, H., and Ji, X. (2021). Kilogram-scale synthesis and functionalization of carbon dots for superior electrochemical potassium storage. ACS Nano *15*, 6872–6885. https://doi.org/10.1021/acsnano.0c10624.

Liu, S., Tian, J., Wang, L., Zhang, Y., Qin, X., Luo, Y., Asiri, A.M., Al-Youbi, A.O., and Sun, X. (2012). Hydrothermal treatment of grass: a low-cost, green route to nitrogen-doped, carbon-rich, photoluminescent polymer nanodots as an effective fluorescent sensing platform for label-free detection of Cu(II) ions. Adv. Mater. *24*, 2037–2041. https://doi.org/10.1002/adma.201200164.

Liu, Z., Zou, H., Wang, N., Yang, T., Peng, Z., Wang, J., Li, N., and Huang, C. (2018). Photoluminescence of carbon quantum dots: coarsely adjusted by quantum confinement effects and finely by surface trap states. Sci. China Chem. *61*, 490–496. https://doi.org/10.1007/s11426-017-9172-0.

Liu, G., Zhao, J., Wang, S., Lu, S., Sun, J., and Yang, X. (2020). Enzyme-induced in situ generation of polymer carbon dots for fluorescence immunoassay. Sens. Actuators. B Chem. *306*, 127583. https://doi.org/10.1016/j.snb.2019.127583.

Meng, T., Wang, Z., Yuan, T., Li, X., Li, Y., Zhang, Y., and Fan, L. (2021). Gram-scale synthesis of highly efficient rare-earth-element-free red/green/blue solid-state bandgap fluorescent carbon quantum rings for white light-emitting diodes. Angew. Chem. Int. Ed. Engl. *60*, 16343–16348. https://doi.org/10.1002/ange.202103361.

Mosconi, D., Mazzier, D., Silvestrini, S., Privitera, A., Marega, C., Franco, L., and Moretto, A. (2015). Synthesis and photochemical applications of processable polymers enclosing photoluminescent carbon quantum dots. ACS Nano *9*, 4156–4164. https://doi.org/10.1021/acsnano.5b00319.

Nekoueian, K., Amiri, M., Sillanpää, M., Marken, F., Boukherroub, R., and Szunerits, S. (2019). Carbon-based quantum particles: an electroanalytical and biomedical perspective. Chem. Soc. Rev. *48*, 4281–4316. https://doi.org/10.1039/c8cs00445e.

Qin, D., Jiang, X., Mo, G., Feng, J., Yu, C., and Deng, B. (2019). A novel carbon quantum dots signal amplification strategy coupled with sandwich electrochemiluminescence immunosensor for the detection of CA15-3 in human serum. ACS Sens. *4*, 504–512. https://doi.org/10.1021/acssensors.8b01607.

Semeniuk, M., Yi, Z., Poursorkhabi, V., Tjong, J., Jaffer, S., Lu, Z.H., and Sain, M. (2019). Future perspectives and review on organic carbon dots in electronic applications. ACS Nano *13*, 6224–6255. https://doi.org/10.1021/acsnano.9b00688.

Shi, Y., Wang, Z., Meng, T., Yuan, T., Ni, R., Li, Y., Li, X., Zhang, Y., Tan, Z., Lei, S., and Fan, L. (2021). Red phosphorescent carbon quantum dot organic framework-based electroluminescent light-emitting diodes exceeding 5% external quantum efficiency. J. Am. Chem. Soc. *143*, 18941–18951. https://doi.org/10.1021/jacs.1c07054.

Sun, Y.-P., Zhou, B., Lin, Y., Wang, W., Fernando, K.A.S., Pathak, P., Meziani, M.J., Harruff, B.A., Wang, X., Wang, H., et al. (2006). Quantum-sized carbon dots for bright and colorful photoluminescence. J. Am. Chem. Soc. *128*, 7756–7757. https://doi.org/10.1021/ja062677d.

Thomson, G.W. (1946). The Antoine equation for vapor-pressure data. Chem. Rev. *38*, 1–39. https://doi.org/10.1021/cr60119a001.

Vasilopoulou, M., Kim, H.P., Kim, B.S., Papadakis, M., Ximim Gavim, A.E., Macedo, A.G., Jose da Silva, W., Schneider, F.K., Mat Teridi, M.A., Coutsolelos, A.G., and bin Mohd Yusoff, A.R. (2020). Efficient colloidal quantum dot light-emitting diodes operating in the second near-infrared biological window. Nat. Photonics *14*, 50–56. https://doi.org/10.1038/s41566-019-0526-z.

Wang, L., Zhu, S.-J., Wang, H.-Y., Qu, S.-N., Zhang, Y.L., Chen, Q.-D., Xu, H.-L., Han, W., Yang, B., and Sun, H.-B. (2014). Common origin of green luminescence in carbon nanodots and graphene quantum dots. ACS Nano *8*, 2541–2547. https://doi.org/10.1021/nn500368m.

Wang, Z., Yuan, F., Li, X., Li, Y., Zhong, H., Fan, L., and Yang, S. (2017). Bright multicolor bandgap fluorescent carbon quantum dots for electroluminescent light-emitting diodes. Adv. Mater. *29*. https://doi.org/10.1149/ma2017-01/12/826.

Wang, L., Li, W., Liu, Y., Guo, H., Lai, J., Han, Y., Li, G., Li, M., Zhang, J., Vajtai, R., et al. (2020). Full-color fluorescent carbon quantum dots. Sci. Adv. *6*, 6772–6779. https://doi.org/10.1126/sciadv.abb6772.

Wareing, T.C., Gentile, P., and Phan, A.N. (2021). Biomass-based carbon dots: current development and future perspectives. ACS Nano *15*, 15471–15501. https://doi.org/10.1021/acsnano.1c03886.

Weetman, C., Bag, P., Szilvasi, T., Jandl, C., and Inoue, S. (2019). CO_2 fixation and catalytic reduction by a neutral aluminum double bond. Angew. Chem. *58*, 10961–10965. https://doi.org/10.1002/ange.201905045.

Xu, Q., Zhou, Q., Hua, Z., Xue, Q., Zhang, C., Wang, X., Pan, D., and Xiao, M. (2013). Single-particle spectroscopic measurements of fluorescent graphene quantum dots. ACS Nano *7*, 10654–10661. https://doi.org/10.1021/nn4053342.

Yuan, F., Yuan, T., Sui, L., Wang, Z., Xi, Z., Li, Y., Li, X., Fan, L., Tan, Z., Chen, A., et al. (2018). Engineering triangular carbon quantum dots with unprecedented narrow bandwidth emission for multicolored LEDs. Nat. Commun. *9*, 2249. https://doi.org/10.1038/s41467-018-04635-5.

Yuan, T., Yuan, F., Li, X., Li, Y., Fan, L., and Yang, S. (2019). Fluorescence–phosphorescence dual emissive carbon nitride quantum dots show 25% white emission efficiency enabling single-component WLEDs. Chem. Sci. *10*, 9801–9806. https://doi.org/10.1039/c9sc03492g.

Zhang, Q.Q., Yang, T., Li, R.S., Zou, H.Y., Li, Y.F., Guo, J., and Liu, X.D. (2018). A functional preservation strategy for the production of highly photoluminescent emerald carbon dots for lysosome targeting and lysosomal pH imaging. Nanoscale *10*, 14705–14711. https://doi.org/10.1039/c8nr03212b.

Zhu, S., Meng, Q., Wang, L., Zhang, J., Song, Y., Jin, H., Zhang, K., Sun, H., Wang, H., and Yang, B. (2013). Highly photoluminescent carbon dots for multicolor patterning, sensors, and bioimaging. Angew. Chem. Int. Ed. Emgl. *52*, 3953–3957. https://doi.org/10.1002/ange.201300519.

STAR★METHODS

KEY RESOURCES TABLE

REAGENT or RESOURCE	SOURCE	IDENTIFIER
Chemicals, peptides, and recombinant proteins		
1,3,5-benzenetricarboxylic acid	Aladdin (Shanghai, China)	CAS: 554-95-0
o-phenylendiamine	Aladdin (Shanghai, China)	CAS: 95-54-5
m-phenylendiamine	Aladdin (Shanghai, China)	CAS: 108-45-2
p-phenylendiamine	Aladdin (Shanghai, China)	CAS: 106-50-3
N,N-dimethylformamide	Aladdin (Shanghai, China)	CAS: 68-12-2
Zinc nitrate hexahydrate	Aladdin (Shanghai, China)	CAS: 10196-18-6
Cadmium nitrate	Aladdin (Shanghai, China)	CAS: 10325-94-7
Cobaltous nitrate hexahydrate	Aladdin (Shanghai, China)	CAS: 10026-22-9
Chromium(III) nitrate nonahydrate	Aladdin (Shanghai, China)	CAS: 7789-02-8
Copper nitrate trihydrate	Aladdin (Shanghai, China)	CAS: 10031-43-3
Ferric nitrate nonahydrate	Aladdin (Shanghai, China)	CAS: 7782-61-8
Diethylenetriamine	Makclin (Guangzhou, China)	CAS: 111-40-0
Mercuric nitrate	Makclin (Guangzhou, China)	CAS: 10045-94-0
Nickel(II) nitrate hexahydrate	Makclin (Guangzhou, China)	CAS: 13478-00-7
Uranyl(VI) nitrate hexahydrate	Beijing HWRK (Beijing, China)	CAS: 13520-83-7
Other		
UV chip	Ruibaoguang Technology Company (Shenzhen, China)	NA

RESOURCE AVAILABILITY

Lead contact

Further information and requests for resources should be directed to and will be fulfilled by the lead contact, Jianqiao Xu (xujq27@mail.sysu.edu.cn).

Materials availability

All unique/stable reagents generated in this study are available from the lead contact with a completed materials transfer agreement.

Data and code availability

All data are available in the paper and in supplemental information, and/or from the corresponding authors upon reasonable request. This paper does not report original code.

EXPERIMENTAL MODEL AND SUBJECT DETAILS

This work did not need any unique experimental model.

METHOD DETAILS

Preparation of CQDs

For the DETA originated blue CQDs (d-bCQDs), BTCA (0.015 g) and DETA (120 μL) were placed in a 20 mL glass bottle. DMF (12 mL) and H_2O (1.4 mL) were added. Then, the bottle was sealed with a TFPE septum lined steel cap, and heated up to 85°C and kept at this temperature for 6 h. Subsequentlly, the as-synthesized d-bCQDs solotion was obtained with strong blue light emission under UV light (365 nm). Similary, the other CQDs were prepared by replacing DETA with oPDA, mPDA, or pPDA. It should be noted, the masses of oPDA, mPDA, and pPDA were all controlled at 0.015 g. By referring to previous work, the as-synthesized solutions can be purified via silica column chromatography (Ding et al., 2016; Alaş and Genç, 2021; Jia et al.,

2019). It was found the mixture components were more beneficial on the applications of sensing metal ions. The d-bCQDs, *m*-bCQDs, and *o*-bCQDs were directly used in following studies, but the treated *p*-rCQDs solution was diluted to 20–50 times before use.

Preparation of CQDs with different ratios of precursors

For the *o*-phenylenediamine (oPDA) originated *o*-bCQDs, BTCA (0.015 g) was separately mixed with oPDA (0.005, 0.010, 0.015, 0.020, 0.025 g) in five 20 mL glass bottle. DMF (12 mL) and H2O (1.4 mL) were added. Then, the bottle was sealed with a TFPE septum lined steel cap, and heated up to 85°C and kept at this temperature for 6 h. Subsequentlly, the as-synthesized *o*-bCQDs solution was obtained. Similary, the other CQDs were prepared by replacing oPDA with different contente of DETA, mPDA, or pPDA.

QY measurement

The absolute QY values were measured from the ratios between photons emitted and absorbed by CQDs. The measurements were performed using an integrating sphere attached to Edinburgh FLS 1000. The excitation light was set at 360 nm with using a 450 W Xenon lamp. The CQDs solutions were placed in a UV quarts cuvette with a light path of 10 mm. The solvent DMF filled in the quarts cuvette was used as a blank sample for reference. The spectral correction curve that related to the sensitivity of the monochromator, detector, sphere coating, and optics to wavelength was provided by Edinburgh Instruments.

LED fabrication

All LEDs were fabricated with similar preparation process by referring previously reported work (Wang et al., 2020). Taking WLED as an example, 200 μL of the CQDs solution was mixed with the solution of polydimethylsiloxane precursors (Dow Corning 184 glue dissolved in cyclohexane, 0.1 g mL^{-1}). Then, the mixture was stirred for 10 min (1000 rpm) and added dropwise to the UV chip. Subsequently, the device was dried in an oven at 50°C for 30 min.

Procedures for sensing metal ions

The metal salt stock solutions were prepared in DMF (concentration 10 mg L^{-1}). The 100 μL of the aforementioned CQDs solution and an aliquot of metal salt solution (200 μL) were mixed. The mixture was diluted to a final volume of 700 μL by DMF. Subsequentlly, the photoluminescence spectra were collected under the maximum excitation wavelength.

Reaction pressure calculation

In this work, a series of CQDs was prepared in glass bottles with the reaction temperature at 85°C. We made a crude estimate of the reaction pressure. In a sealed glass bottle, the volumes of the gas and liquid in the bottle was considered unchanged as the reaction temperature far below the boiling point of the solvent (152.8°C for DMF and 100°C for H_2O under 1 atm). The real pressure in the bottle was the sum of the gas pressure and vapor pressures under heating process.

First, the gas pressure was estimated using the equation:

$$(P_1V_1)/T_1 = (P_2V_2)/T_2$$

where P, V, T denoted the pressure, volume and temperature for gas in the glass bottle, respectively. The initial P_1 was about 1 atm at 25°C (298.15 K). When the reaction temperature reached 85°C (358.15 K), the presurre in the glass bottle was calculated to be about 1.20 bar. Second, the vapor pressures were calculated using the Antoine equation (Thomson, 1946):

$$lgP = A - B/t + C$$

where A, B and C are the empirical constant. T and P denoted as the parameters of Celsius temperature (°C) and vapor pressure (mmHg), respectively. For H_2O, the parameters of A, B and C are 7.96681, 1668.210 and 228.000 in the temperature range of 60–150°C, respectively. When the reaction temperature reached 85°C (358.15 K), the vapor pressure of H_2O in the glass bottle was calculated to be 0.56 bar. For DMF, the parameters of A, B and C are 6.99608, 1437.840 and 199.830 in the temperature range of 60–350°C, respectively. When the reaction temperature reached 85°C (358.15 K), the vapor pressure of DMF in the glass bottle was calculated to be 0.12 bar. Therefore, the whole pressure in the reacting environment was calculated to be 1.88 bar.

QUANTIFICATION AND STATISTICAL ANALYSIS

Figures represent averaged or representative results of multiple independent experiments. Analyses and plots were performed with Origin.

ADDITIONAL RESOURCES

There are no additional resources needed to be declared in this manuscript, additional requests for this can be made by contacting the lead contact.